DOI: 10.21062/mft.2023.091 http://www.journalmt.com

Effect of PWHT of X6Cr-NiNbN 25-20 Steel on the Evolution of the Sigma Phase during Creep Exposure at 700 °C

Jakub Rehorek (0009-0008-4587-5296)[1, 2]
[1]Faculty of Materials Science and Technology, VSB Technical University of Ostrava. 17. listopadu 2172/15, 708 00 Ostrava-Poruba. Czech Republic: jakub.rehorek@vsb.cz.
[2]Research Centere Rez. Hlavni 130, 250 68 Husinec-Rez Czech Republic. Email: jakub.rehorek@cvrez.cz.

Superheaters and reheaters made of heat–resistant austenitic steels are being replaced in existing fossil fuel power plants to operate at Advanced Ultra Super Critical (A-USC) parameters of steam. Newly developed and used high nickel content austenitic steels, such as in X6Cr NiNbN 25-20, are predicted to significantly suppress the precipitation of a hazardous σ-phase during long-term creep exposure. The σ-phase causes premature failure of the component during creep, which is usually supported by a local change in hardness in the case of welded assemblies. Experimental results show that PWHT significantly improved reduction of area. However, for the PWHT specimen with a shorter exposure time of 15,712 hours, there was an acceleration in the precipitation of σ-phase particles during creep at 700 °C compared to the specimen in the AW state, after 20,557 hours.

Keywords: HR3C, Weld joint, σ-phase, Creep, PWHT, A-USC

1 Introduction

The worldwide demand for lower electricity prices and, at the same time, lower emissions are putting pressure on increasing the thermal efficiency of existing, revitalised and/or under construction fossil power plant units [1]. This can be achieved by increasing the steam parameters, i.e. the temperature and pressure of the steam at the inlet of the steam turbines [2]. However, the use of high parameter steam is subject to the availability of suitable construction materials. Grades of heat resistant austenitic steels developed in recent decades have already been deployed in a modernised power plant in the Czech Republic [3]. For these steels, no relevant data are available on their degradation during long-term operation, especially for their welded joints. However, this information is very important for the prediction of the lifetime of the components in service. Among the steels with very good creep resistance is the 25Cr-20Ni based austenitic steel HR3C [X6Cr-NiNbN 25-20] [4]. Exposed parts of fossil power plant boiler components with steam parameters USC 600/620 °C and 28.5 MPa, as well as components for new advanced units with steam parameters A-USC 700 °C and up to 38 MPa, are produced and operated from this steel [5].

The precipitation of the σ-phase is faster in the stabilized heat-resistant austenitic steels grades than in the other grades. Minami et al. [6] observed σ-phase precipitation in most grades of austenitic heat-resistant austenitic steels: type AISI 304, 316, 321 and 347. The σ-phase precipitation after different times (as early as 1000 hours at 700 °C for 347 and 321), but for 304, 316 and Tempaloy-A1 the σ-phase was detected in significant amounts after 10 000 hours. According to experimental results, the presence of σ-phase leads to a significant loss of reduction of area and premature rupture due to the presence of coarse particles along the austenitic grain boundaries. Post-weld heat treatment (PWHT) results in the dissolution of all secondary phase particles before creep. This paper aims to verify the effect of dissolution annealing on the creep properties and microstructure in relation to the developer of σ-phase of the studied HR3C (X6Cr-NiNbN 25-20) steel weld.

2 Experimental Methods

The evaluation was carried out on completed long-term creep tests after rupture. The long-term rupture creep tests were carried out in accordance with ISO 204 [7]. Testing was carried out using uniaxial tension. All tests were carried out in the creep laboratory at MATERIAL AND METALLURGICAL RESEARCH, Ltd. Ostrava-Vitkovice. Creep stands with constant load were used as test equipment. The mean testing temperature was set at 700 °C. In addition, two other temperatures were set, i.e. 50 °C above the mean temperature and 50 °C below the selected mean temperature. Creep tests were performed at five stress levels ranging from 100 to 150 MPa. The tests were carried out in air without an inert atmosphere.

The Larson-Miller (L-M) equation was used to process the creep results for the entire series of weld

samples in both the as–welded (AW): Series A and PWHT: Series B states [8]. For the above creep test results, the L-M parameter was determined and the results of the base material (BM) of the experimental material with the homogeneous weld joints which differ in the method post-weld heat treatment were compared.

Colour-tint etching is being widely used again with the development of digitalisation and the associated availability of colour photography [9–11]. Both the Murakami colour etching technique and the interpretation of the phase maps acuired by the backscattered electron diffraction technique in a scanning electron microscope (SEM-EBSD) were used to evaluate the microstructure and determine the σ-phase particle size [12]. The measurements were performer using light optical microscope Zeiss AXIO Observer Z1 and Tescan LYRA3 auto-emission cathode (FEG) microscope equipped with a NordlysNano EBSD detector (oxford Instruments). The surface was prepared by conventional metallographic methods and chemo-mechanically polished for the purposes of the EBSD abalysis. V2A etchant (10 ml HNO_3 + 100 ml HCl + 100 ml H_2O) was used to highlight the grain boundaries and the underlying microstructure. The etching time per one sample was ~10 min. To induce the reaction with σ-phase, Murakami-based colour etchant (30 g $K_3[Fe(CN)_6]$, 30 g KOH and 60 ml H_2O) was used: yellow reaction colour. The etching time per one sample was ~10 seconds.

The results were supplemented by both the measurement of average austenitic grain size according to ASTM E112 [13] by optical microscopy and the assessment of microhardness HV0.5 according to ASTM E384 [14] on a Struers Durascan 70. The microhardness measurements were made in two lines along the full length of the longitudinal axial section through the specimen. The distance between the indentations was constant and was 2.5 lengths of one diagonal of the indentation. The diagonal size of one indentation was ~7 μm.

3 Experimental Material

The HR3C austenitic heat resistant steel (X6Cr NiNbN 25-20) was received in the form of tubes. The exact chemical composition was determined by a combination of wavelength-dispersive X-ray spectrometry (WDS) with appropriate material standards and plasma analysis using equipment LECO CS844 for caron and sulphur and HORIBA EMGA-830 for nitrogen exact analysis. The results of the chemical composition analysis are presented in Table 1. Creep samples were made from the experimental material by machining, the samples were of standard circular type with threaded heads [7]. Table 2 shows the testing parameters and results after creep testing.

Tab. 1 *Chemical composition of the experimental material (wt. %)*

	Melt	C	Cr	Ni	N	Nb	Mn	Co	Si	Mo	Cu	B	V	S	Al	Fe
HR3C	**F122036**	0.059	25.69	19.34	0.283	0.27	1.30	0.514	0.318	0.151	0.067	0.057	0.015	0.005	0.006	bal.

The dimensions of the welded tubes were ø 38 x 6.3 mm. The welds were fabricated using automated orbital welding technology 141 (TIG, GTAW) on Polysoude equipment. The welding was performed "flat". Both tube ends were centred horizontally and did not move during welding. Thermanite 617 was used as an filler material. The diameter of the welding wire was chosen to be 0.8 mm with the trade name BÖHLER UDDEHOLM. Designation EN ISO 18274: S Ni 661 (NiCr22Co12Mo), according to AWS A5.14-05: ERNiCrCoMo-1, according to VdTÜV: Wr.-Nr. 2.4627. Detailed information about the welding process is given in paper [15]. Creep and mechanical properties are drawn from the relevant VdTÜV standard [16]. The exact chemical composition of the basic material of HR3C steel is given in Table 1. Due to the high thermal expansion of austenite and the associated risk of hot cracking, the heat input was limited. The heat input Q for the individual weld layers was therefore selected in the range of 1100 to 1900 $J \cdot mm^{-1}$. The interpass temperature did not exceed 150 °C [15].

Tab. 2 *Creep test parameters and results*

	State	Exposure (°C)	Stress (MPa)	Time to rupture (hours)	Reduction of area (%)
A1	PWHT	700	110	6,958	-
A2	PWHT	700	90	15,712	-
B1	AW	700	120	3,967	6.7
B2	AW	700	70	21,557	11.7
C1	AW	650	110	37,672	1.6

After the welding, one of the tube was further exposed to the PWHT. The second tube of the series was left in the AW state without any further heat treatment. The heat treatment mode included a dissolution annealing with heating to a temperature of 1230 ± 10 °C, stabilization at temperature and a hold time of at least 15 min. Subsequently, rapid cooling in water was performed. After welding, creep specimens were fabricated from the A-series and B-series tubes in the longitudinal direction across the circumferential weld. ("cross-weld" creep specimens). The macrostructure of the blank before the production of the cross-weld samples is shown in Fig. 1.

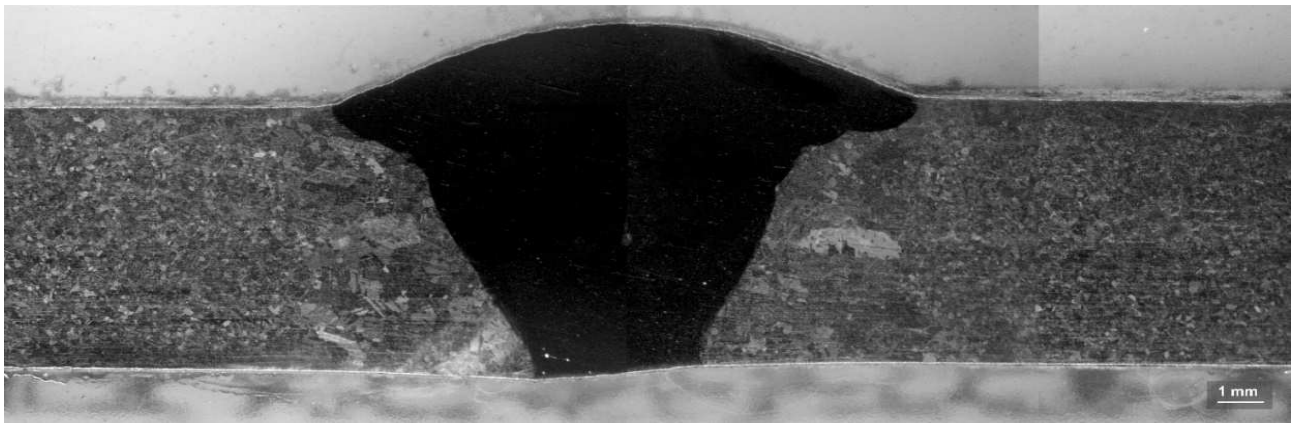

Fig. 1 *LOM-BF image of the cross-sectional structure of the X6CrNiNbN 25-20 welded tube after PWHT*

The study of σ-phase evolution by Murakami colour etching was carried out on A1 and A2 specimens to which PWHT was applied. Colour etching to visibility of σ-phase was also performed on B1 and B2 specimens, these specimens were left in the AW state. Creep tests were performed on both series at 700 °C. To complement the results, especially the particle size distribution of the σ-phase, sample C1 which was not heat treated after welding was included in the σ-phase evaluation. The creep test for sample C1 was performed at 650 °C, as opposed to samples A1-2 and B1-2. The Larson-Miller equation (Eq. 1) was used to interpret the creep properties of the completed creep tests [8].

$$P_{LM} = T(C + log_{tr}) = \frac{Q}{2.3R} \qquad (1)$$

Where:

P_{LM}…Larson-Miller's correlation parameter [-],

t_r…Time to rupture [h],

T…Temperature [K],

C…Material constant, independent of temperature [-],

Q…Activation energy [J·mol^{-1}],

R… Gas constant [8,314 J·mol^{-1}·K^{-1}].

4 Results

The converted results of the completed creep tests are documented in Fig. 2, where dark symbols represent the base material (BM) and light symbols represent the homogeneous weld joint (C-W).

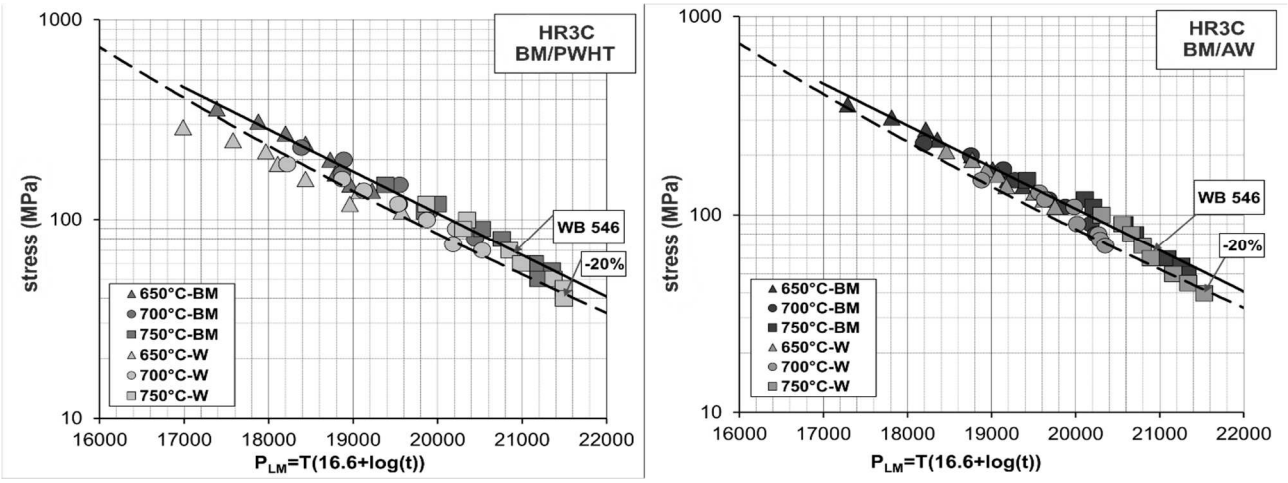

Fig. 2 *Results of creep to rupture tests as a function of stress on P_{LM} BM of HR3C steel and homogeneous weld of HR3C steel in AW state (right) and after PWHT (left) at 650, 700 and 750 °C*

The full lines in Fig. 2, labeled WB 546, represent the average values of the creep strength of HR3C steel according to reference [16]. The dashed lines correspond to the lower -20% tolerance limit of the average creep strength values of HR3C steel.

The results confirmed good creep resistance of the tested tubes and their welded joints. It is worth noting that for the Serie A (PWHT) weld, the highest applied stresses and therefore shorter time to rupture at 650 °C resulted in a deviation from the mean calculated creep strength and significantly below the lower -20% tolerance limit of the average creep strength values of HR3C steel. This trend gradually disappeared with decreasing applied stress (Fig. 2, left). The B series weld (AW) showed very good agreement with the mean calculated creep strength and was within the -20% tolerance of the mean creep strength of HR3C steel.

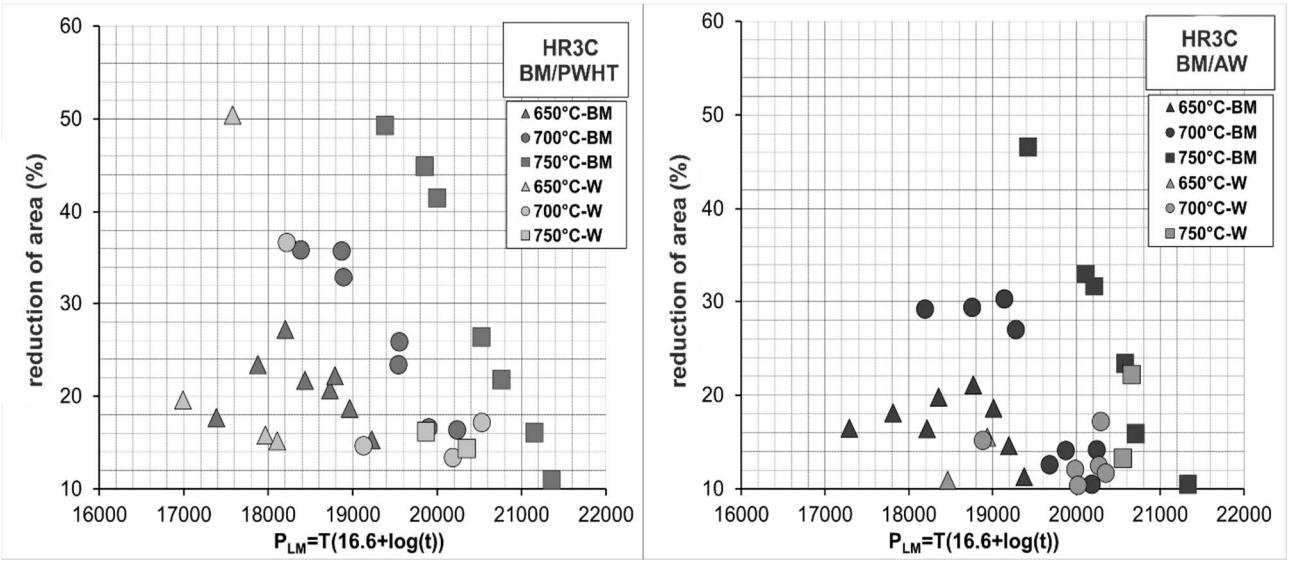

Fig. 3 *Dependence of fracture contraction on P_{LM} BM of HR3C steel and homogeneous weld of HR3C steel in AW state (right) and after PWHT (left) at 650, 700 and 750 °C*

The danger of σ-phase precipitation in the X6Cr NiNbN 25-20 austenitic steel does not lie in the reduction of creep strength, but in the depletion of plasticity and matrix embrittlement [17]. This phenomenon can be clearly seen in Fig. 3, which show the dependence of the reduction of area on the Larson-Miller parameter both in the studied steel in BM and more significantly in the weldments. Fig. 3 on the right shows a very dramatic decrease in reduction of area for the B-series (AW) state as opposed to the A-series (PWHT) weld.

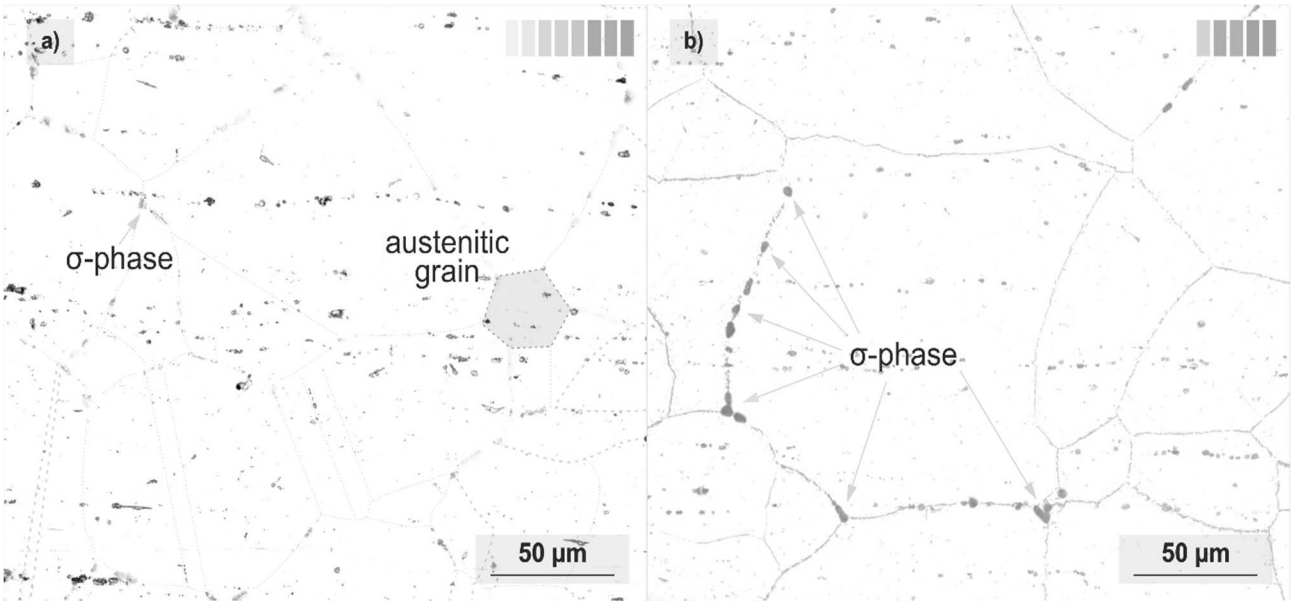

Fig. 4 *Colour etching for σ-phase imaging in Murakami, HE3C steel exposed at 700 °C, a) sample A1: 6,958 hours in PWHT state, b) sample B1: 3,967 hours in AW state*

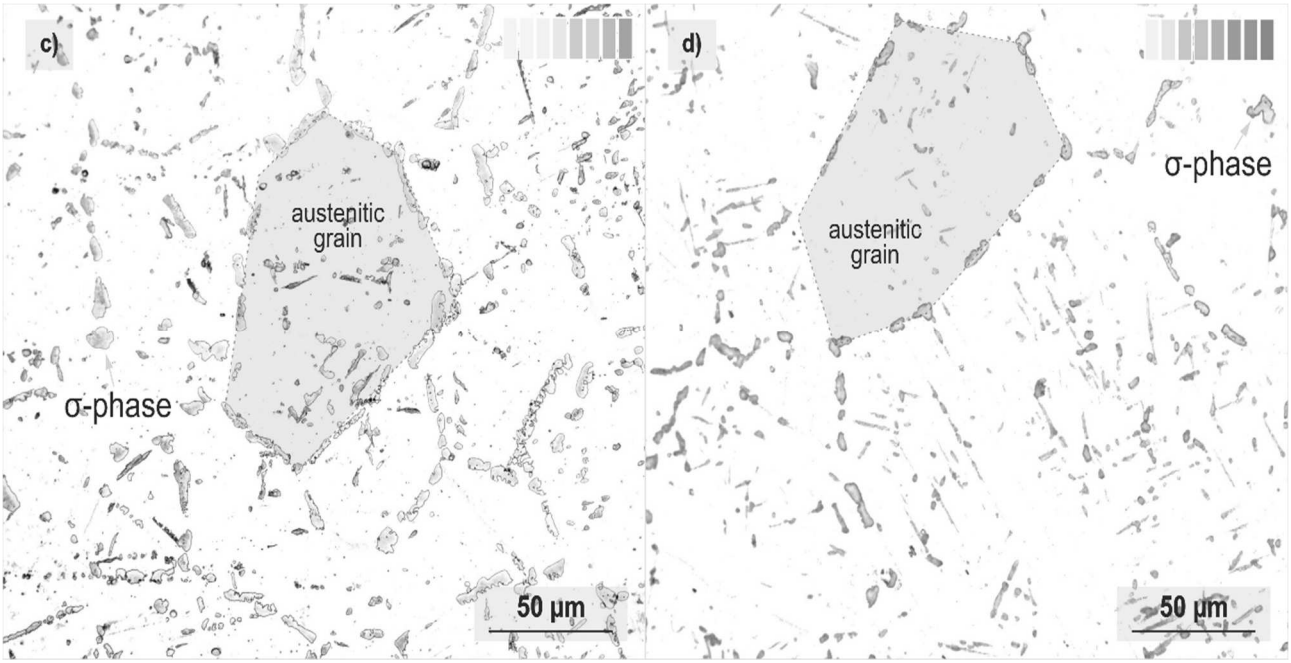

Fig. 5 *Colour etching for σ-phase imaging in Murakami, HR3C steel exposed at 700 °C, c) sample A2: 15,712 hours in the PWHT state, d) sample B2: 21,557 hours in the AW state*

In Fig. 4 and 5, the distribution of the σ-phase particles in the microstructure of all the studied samples of HR3C steel can be observed. The σ-phase particles in Murakami are coloured from light yellow (particles above 3 µm) to dark brown (particles up to 1 µm in size). The resulting yellow-brown colour depends on the particle size of the σ-phase and the total etching time. The range of colours can be limited to dark shades of brown only or to black only if the particle size is 500 nm or less and the etching time is more than 10 sec. The most common colours after etching for σ-phase particles in Murakami for a given sample is shown in the upper right corner of Fig. 4 and Fig. 5. The dashed lines highlight the network of austenitic grain boundaries. Selected grains are highlighted in transparent red for illustrative purposes.

The results of the measurements of the average austenitic grain size and σ-phase particle size and the determination of the microhardness HV0.5 are shown in Table 3.

Tab. 3 *Measurement results of average particle size of σ-phase, austenitic grain size and average microhardness HV0.5 in the non-heat treated base material*

	Average σ-phase particle size (µm)	**Austenitic grain size (µm)**	**Microhardness HV0.5**
A1	3.4 ± 0.2	87 ± 2.3	236 ± 6
A2	8.7 ± 0.4	96 ± 1.9	245 ± 8
B1	4.2 ± 0.3	90 ± 2.4	240 ± 5
B2	5.2 ± 0.7	89 ± 1.6	246 ± 9

From the results in Table 3, it can be seen that the largest average σ-phase particle size was observed for sample A2 after 15,712 hours in the PWHT state, while the smallest was observed for sample A1 after 6,958 hours also in the PWHT state. The results of σ-phase particle size measurements obtained by light optical imaging were further supplementd by SEM-EBSD phase analysis. Both methods are in very good agreement with the results of average σ-phase particle size evaluation. Moreover, it can be seen that the size of the σ-phase precipitates varies greatly depending on the distance of the area of interest from the weld in the longitudinal section of the cross-weld samples. For this reason, a total of five positions from the fusion boundary (FB) through the heat affected zone (HAZ) to the unaffected base material are shown in Fig. 6 below.

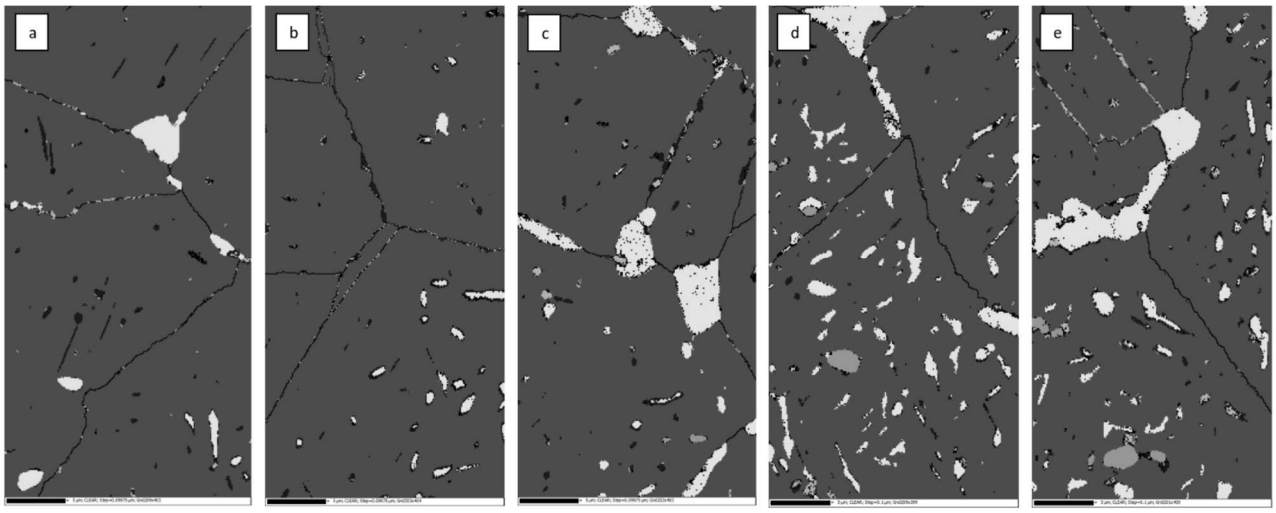

Fig. 6 *EBSD map of specimen C1, phase cotrast of HR3C steel after creep exposure at 650 °C with time to rupture of 37,672 hours. a) FB/HAZ root of weld, b) HAZ/BM 2 mm from FB, c) HAZ/BM 3 mm from FB, d) HAZ/BM 4 mm from FB, e) HAZ/BM 5 mm from FB. The colours indicate the presence of phases: austenite (red), σ-phase (yellow), $M_{23}C_6$ (dark blue), M_6X (blue) and Z-phase (green)*

In Fig. 6, the σ-phase is marked in yellow with an area fraction of 7 ± 2 % and austenite with an area fraction of 95 ± 4 %. The remaining indexations are $M_{23}C_6$, M_6X and Z-phase (modified Z-phase). Very coarse σ-phase particles can be observed at grain boundaries in the peripheral parts of the HAZ (Figs. 6c and 6e) whereas finer σ-phase particles can be observed to be present within the austenitic grains intragranulary in the HAZ (Fig. 6d). In Fig. 6a and 6b, a large fraction of minority phase particles are dissolved into the matrix due to welding.

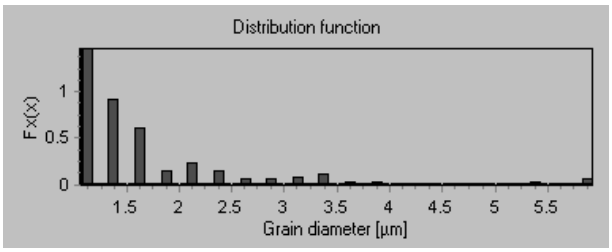

Fig. 7 *Distribution function of the σ-phase particle sizes in the C1 specimen, averaged over the entire length of the axial longitudinal section from the HZ to the head of the creep test specimen*

The distribution function (Fig. 7) shows that the largest number of particles is in the interval from 0.5 to 1 μm. The distribution function has a smooth profile with a local maximum in the interval 3.5 to 4.5 μm. The measured reduction of area values can be directly related to the toughness of the steel, since the σ-phase obviously changes the reduction of area properties. Both tested pipes showed a decrease in reduction of area as a function of σ-phase content compared to samples without σ-phase (shorter exposure time). The effect of PWHT did not result in such a significant decrease in reduction of area in the case of Series B (AW). The stress results on the L_{MP} show that the creep properties of the Series A (PWHT) welds exhibited a lower level of refractoriness than that of the Series B (AW).

5 Conclusion

Formation of σ-phase particles is promoted by elements like chromium, niobium, titanium and molybdenum [12, 18]. Silicon also promotes and accelerates its formation [19]. Coarse particles of this phase facilitated the formation and interlinking of creep cavities, leading to creep rupture. Coarse σ-phase particles contributed significantly to relatively poor creep ductility of the cast investigated after long-term creep exposure.

The measurements of the average σ-phase particle size showed that, although the structure was optimized after PWHT (good reduction of area), the growth of the σ-phase particle size was accelerated during creep for sample A2 with a time to rupture of 15,712 hours with PWHT applied, compared to sample B2 with a time to rupture of 21,557 hours in the AW state. The σ-phase particles were observed along the grain boundaries, mainly at the triple points, and also as smaller coagulated particles intragranular inside the austenite grains. None of the studied samples contained σ-phase particles with a critical particle size of ~10 μm where premature failure of the component during operation is imminent.

There is a decrease in reduction of area as σ-phase precipitation develops. The recalculated results of the reduction of area dependence on P_{LM} clearly showed a dramatic decrease in reduction of area with increasing temperature and time to rupture for the weld without heat treatment applied immediately after welding.

Acknowledgement

This publication was prepared with the support of the Technology Agency CR in the THETA Programme within the project: TK03020055. The presented results were obtained using the CICRR infrastructure, which is financially supported by the Ministry of Education, Youth and Sports – project LM2023041. The presented work has been realized within Institutional Support by Ministry of Industry and Trade of the Czech Republic.

References

[1] MASUYAMA, F. (2001). History of power plants and progress in heat resistant steels. In: *JSIT International*, Vol. 41, No. 6, pp. 612 – 625. Japan. ISSN 0915-1559

[2] KOLLOVÁ, A., PAUEROVÁ, K. (2022). Superalloys – Characterization, Usage and Recycling. In: *Manufacturing Technology*, Vol. 22, No. 5, pp. 550 – 557. Slovak Republic. ISSN 2787-9402.

[3] ŠEREŠOVA, M., ŠTEFANICA, J., VITVAROVÁ, M., et al. (2020). Life Cycle Performance of Various Energy Sources Used in the Czech Republic. In: *Energies*, Vol. 13, No. 21, 5833 p. Czech Republic. ISSN 1996-1073.

[4] ABE, F. (2015) Research and Development of Heat-Resistant Materials for Advanced USC Power Plants with Steam Temperatures of 700 °C and Above. In: *Engineering*, Vol. 1, No. 2, pp. 211 – 224. Japan. ISSN 2095-8099.

[5] DI GIANFRANCESCO, A. (2017). The fossil fuel power plants technology. *Materials for Ultra-Supercritical and Advanced Ultra-Supercritical Power Plants*, pp. 1 – 49. Italy. ISBN 978-0-08-100552-1.

[6] MINAMI, Y., KIMURA, H., IHARA Y. (1986). Microstructural changes in austenitic stainless steels during long-term aging. In: *Materials Science and Technology*. Vol. 2. Japan. ISSN 795-806.

[7] International Organization for Standardization. (2009). *Metallic materials – Iniaxial creep testing in tension – Method of test*. Switzerland. ISO Standard No. 204:2009.

[8] LARSON, F.R., MILLER, J. (1952). Time-Temperature Relationship for Rupture and Creep Stresses. In: *Transaction of ASME*, Vol. 74, pp. 765 – 771.

[9] VAŠKO, A., BELAN, J., TILLOVÁ, E. (2020). Use of colour etching in the structural analysis of graphitic cast irons. In: *Manufacturing Technology*, Vol. 20, No. 6, pp. 845-848. Slovak Republic. ISSN 2787-9402.

[10] WEISS, V., SVOBODOVÁ, J. (2015). The Use of Colour Metallography and EDS for Identification of Chemical Heterogeneity of Selected Aluminium Alloys Copper and Zinc Alloyed. In: *Manufacturing Technology*, Vol. 15, No. 6, pp. 1048-1053. Czech Republic. ISSN 2787-9402.

[11] STŘIHAVKOVÁ, E., WEISS, V. (2012). The Identification of the structures new type Al-Si-Mg Ca alloys with different Ca content using of the color metallography. In: *Manufacturing Technology*, Vol. 12, No. 2, pp. 248-251. Czech Republic. ISSN 2787-9402

[12] BARCIK, J. (1988). Mechanism of σ-phase precipitation in Cr-Ni austenitic steels. In: Materials Science and Technology, Vol. 4, No. 1, pp. 5 – 15.

[13] American Society for Testing and Materials. (2021). *Standard Test Methods for Determining Average Grain Size*. United States of America. ASTM Standard No. E112-13(2021).

[14] American Society for Testing and Materials. (2022). *Standard Test Method for Microindentation Hardness of Materials*. United States of America. ASTM Standard No. E384-22.

[15] POMIKALEK, L., HERMANOVA, S., DOBROVODSKA, L. (2013). Effect of Welding on the Properties of HR3C, Super 304H, TP347HFG and P92 Steels. In: *METAL 2014*, Vol. 23. Czech Republic. ISSN 2694-9296.

[16] Verband Der Technischen Überwachungs-Vereine e.V. (2009). *VdTÜV Werkstoffblatt 546 - Warmfester Walz und Schmiedestahl X6CrNiNbN25-20*, 1.4952, 6 p. Germany.

[17] KUBON, Z., STEJSKALOVA, S., KANDER, L. (2017). Effect of Sigma Phase on Fracture Behavior of Steels and Weld Joints of Components in Power Industry Working at Supercritical Conditions. In: *Austenitic Stainless Steels - New Aspects*, 218 p. (InTech). Czech Republic. ISBN 978-953-51-3701-6.

[18] SOURMAIL, T. (2001). Precipitation in creep resistant austenitic stainless steels. In: *Materials Science and Technology*. Vol. 17, No. 1, pp 1 – 14. United Kingdom. ISSN 0267-0836, 1743-2847.

[19] LEE, Ch., ROH, S., LEE, Ch., et al. (2018). Influence of Si on sigma phase precipitation and pitting corrosion in superaustenitic stainless steel weld metal. In: *Materials Chemistry and Physics*. Vol. 207, pp 91 – 97. Republic of Korea. ISSN 0254-0584.